Observation of strong magnetoelastic coupling in a first-order phase transition of CrOCl

Joachim Angelkort, Alexander Wölfel, Andreas Schönleber, and Sander van Smaalen*
Laboratory of Crystallography, University of Bayreuth, 95440 Bayreuth, Germany

Reinhard K. Kremer
MPI for Solid State Research, Heisenbergstrasse 1, 70569 Stuttgart, Germany

(Received 2 July 2009; revised manuscript received 11 September 2009; published 20 October 2009)

The phase transition of CrOCl toward a state of antiferromagnetic order below $T_N=13.5$ K has been identified as a first-order phase transition. The transition is accompanied by a lattice and structural distortion toward a twofold, 2**b** nuclear superstructure with **a**-axis unique monoclinic symmetry, as evidenced by temperature-dependent x-ray diffraction experiments. Magnetic-susceptibility and magnetization measurements indicate a transition with strong magnetoelastic coupling to a uniaxial antiferromagnet with ordered moments along **c**. A second transition is discovered at $T_c \approx 27.2$ K that is presumably of purely magnetic origin and might indicate the formation of an incommensurate magnetic superstructure. The different behaviors of TiOCl, VOCl, and CrOCl are the result of the different symmetries of the filled $3d$ orbitals, which lead to different exchange interactions on the MO double layers of these isostructural compounds.

DOI: 10.1103/PhysRevB.80.144416 PACS number(s): 61.50.Ks, 61.66.Fn, 75.30.Kz

I. INTRODUCTION

TiOCl has recently attracted attention because of the presence of quasi-one-dimensional $S=1/2$ magnetic chains of Ti atoms, which are responsible for the development of a spin-Peierls state below $T_{c1}=67$ K.[1,2] The low-dimensional character of the magnetic interactions in TiOCl is the result of the presence of the single d electron of Ti^{3+} in the $3d_{x^2-y^2}$ orbital, which then gives rise to a large direct exchange along the chains of metal atoms but allows only weak magnetic exchange between the chains.[3] Several compounds MOCl (where M is a $3d$ transition metal) are known to be isostructural to TiOCl at room temperature.[4–7] They differ from each other in the number of d electrons on the M^{3+} atom. Different phase diagrams may be expected and have indeed been observed.[8–10] Compounds MOCl are thus of interest because variation in the element M allows the magnetic interactions to be varied on otherwise equal lattices.

Isostructural compounds MOX (M=Ti,V,Cr,Fe;X=Cl, Br) crystallize in the FeOCl structure type with space group $Pmmn$ and lattice parameters $a=3.8638(2)$, $b=3.1793(1)$, and $c=7.7157(3)$ Å for CrOCl at room temperature.[4] The crystal structures consist of MO double layers sandwiched between layers of halogen atoms which stack along the lattice direction **c** (Fig. 1). Another view of the structure is that of ribbons MOX perpendicular to **a**. Within each ribbon a chain of metal atoms runs along **b**. The short M-M distances ($d=3.179$ Å) along these chains allow direct exchange interactions between electrons on neighboring atoms.[3] Direct exchange between Ti atoms has been discussed as the reason for the unusual phase diagrams of TiOCl and TiOBr. However, the shortest M-M bond ($d=3.006$ Å) is between ribbons, i.e., between Cr1 and Cr3 in Fig. 1. Depending on the symmetry of the filled d orbitals, direct exchange between ribbons as well as superexchange between ribbons and superexchange along **a** must be considered.

In TiOCl and TiOBr a spin-Peierls transition has been observed inducing a lowering of the orthorhombic to monoclinic symmetry. The low-temperature spin-Peierls phases in TiOCl and TiOBr have **a**-axis unique monoclinic symmetry.[2] In addition both compounds exhibit an intermediate phase between T_{c1} and T_{c2}—with $T_{c2}=90$ K for TiOCl—which is incommensurately modulated with **c**-axis unique monoclinic symmetry.[11–13] Recently it was found that VOCl displays an **c**-axis unique monoclinic lattice distortion below $T_N=80.3$ K, which supports antiferromagnetic (AFM) order with a twofold magnetic superstructure.[14,15] The formation of this phase can be explained by the filling of two $3d$ orbitals by the two d electrons of V^{3+}.

CrOCl was reported to develop AFM order at low temperatures with a fourfold magnetic superstructure.[8] Here we report the temperature dependence of the anisotropic magnetic susceptibility, which indicates that ordered magnetic moments are parallel to **c**. X-ray diffraction experiments reveal that the magnetic transition to the AFM state is accompanied by an **a**-axis unique monoclinic lattice distortion. The transition to the magnetically ordered state is a first-order transition and it is accompanied by a structural distortion toward a twofold superstructure. By combining temperature-dependent and field-dependent magnetization and specific-heat measurements we arrive at a proposal of the (H,T)

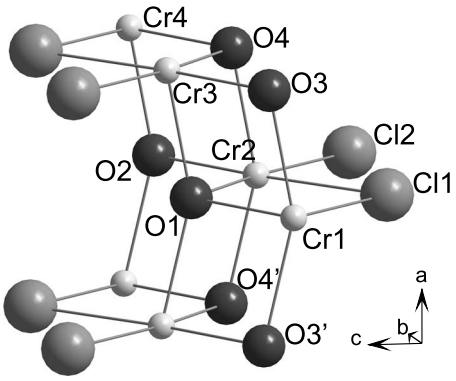

FIG. 1. Crystal structure of CrOCl.

phase diagram of CrOCl. The differences in phase diagrams of different compounds *M*OCl are discussed in view of the different numbers of *d* electrons of the metal atoms.

II. EXPERIMENT

Single crystals of CrOCl were grown in evacuated quartz-glass ampoules by gas transport according to published procedures.[4,16] Stoichiometric amounts of Cr_2O_3 (Alpha, 99.997% purity) and $CrCl_3$ (Alpha, 99.9%) were mixed with $HgCl_2$ as transport agent and placed in a sealed and evacuated quartz-glass ampoule. The ampoule was heated for five days in a temperature gradient of 1223 K (educt side) to 1123 K (product side). CrOCl formed at the product side of the ampoule as greenish platelike crystals of up to several millimeter in length. The sample also contained smaller amounts of a dark green powder (Cr_2O_3) on the educt side and $CrCl_3$ on the product side.

Magnetic susceptibilities at constant field and varying temperature and magnetizations at constant temperature and varying field of a single crystal of 0.45 mg were measured in a Quantum Design Magnetic Properties Measurement System (MPMS) squid magnetometer with the magnetic field oriented either parallel or perpendicular to **c**. Heat capacities of the same crystal were determined with the magnetic field oriented parallel to **c** in a Quantum Design Physical Properties Measurement System (PPMS) employing the relaxation method.

A crystal of dimensions $0.15\times0.05\times0.005$ mm^3 was selected for x-ray diffraction experiments using synchrotron radiation of wavelength 0.71000 Å. The crystal was glued to a carbon fiber that was attached to the cold finger of a closed-cycle helium cryostat mounted on the Huber four-circle diffractometer at beamline D3 of Hasylab at DESY, Hamburg, Germany, equipped with a scintillation detector. Diffraction was measured at selected temperatures between 8 K and room temperature.

III. RESULTS

A. Magnetic susceptibility and magnetization

Above ~175 K the magnetic susceptibilities follow a Curie-Weiss law according to (Fig. 2)

$$\chi_{mol} = \frac{C}{T-\Theta} + \chi_{dia} \qquad (1)$$

with a Curie constant $C=1.825(9)$ cm^3 K/mol, equivalent to an effective magnetic moment $\mu_{eff}=3.82(1)\mu_B$, in good agreement with previous measurements.[4] When fitting Eq. (1) to the data, we fixed the diamagnetic contribution to $\chi_{dia}=-49\times10^{-6}$ cm^3/mol, corresponding to the sum of the diamagnetic increments of the constituting elements in their respective oxidation states according to Selwood,[17] Cr^{3+}: 11×10^{-6} cm^3/mol; O^{2-}: 12×10^{-6} cm^3/mol; Cl^-: 26×10^{-6} cm^3/mol. The effective moment is in good agreement with the value expected for a $3d^3$ electronic configuration with spin-only $S=3/2$ state of the Cr^{3+} ion and a *g* factor of $g\approx1.97$ somewhat reduced from the free-electron *g* factor due to spin-orbit coupling effects.[18] The Curie-Weiss temperature is positive and amounts to $\Theta=19.2(5)$ K, indicating predominant ferromagnetic exchange interaction.

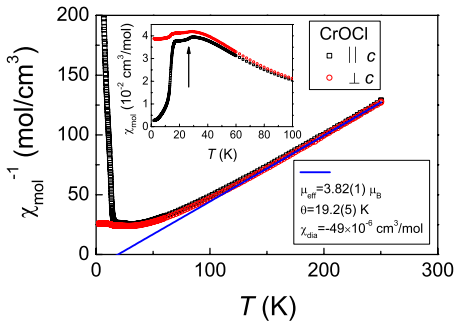

FIG. 2. (Color online) Magnetic susceptibility of CrOCl measured in a magnetic field of 0.1 T parallel and perpendicular to **c**. The (blue) solid line represents a fit of the Curie-Weiss law [Eq. (1)] to the data at temperatures $T>175$ K (see text). The small but finite value of $\chi_\parallel$ for $T\to0$ is attributed to a slight misalignment of the crystal. The arrow in the inset indicates a weak anomaly near $T_c\approx27.2$ K.

Below about 80 K the susceptibilities measured with fields parallel and perpendicular to the **c** axis increasingly deviate from each other. A broad maximum appears at ~30 K for both directions of the field. Below ~14 K $\chi_\parallel$ drops almost to zero while $\chi_\perp$ levels off at a value of 3.88×10^{-2} cm^3/mol indicating long-range AFM ordering in agreement with previous findings.[8] The splitting of parallel and perpendicular susceptibilities is consistent with the notion of an easy-axis antiferromagnet with the easy axis along or close to the crystallographic **c** axis.

Onset of AFM long-range ordering below ~14 K is marked by an anomaly at 13.9(1) K in the specific heat (C_p) measured on the same crystal as used for the determination of the magnetic susceptibilities. An additional, split anomaly of about the same magnitude is observed at 26.7 and 27.8 K (Fig. 3).

Magnetization experiments with the magnetic field applied along the easy axis revealed a spin-flop transition at a flop field $H_{SF}=3.2(1)$ T (Fig. 4). A hysteresis is observed between the magnetization measured with increasing and decreasing fields. The derivative dM/dH clearly reveals the splitting of the transition measured with increasing and de-

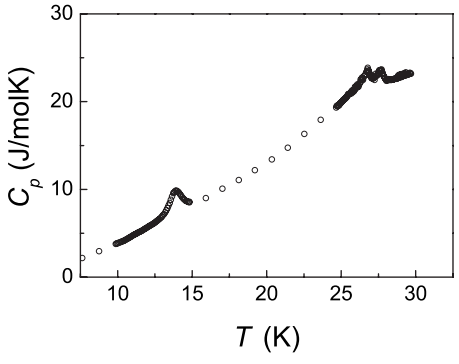

FIG. 3. Temperature dependence of the specific heat C_p of CrOCl. Anomalies are clearly revealed at 13.9(1) K and at 26.7 and 27.8 K.

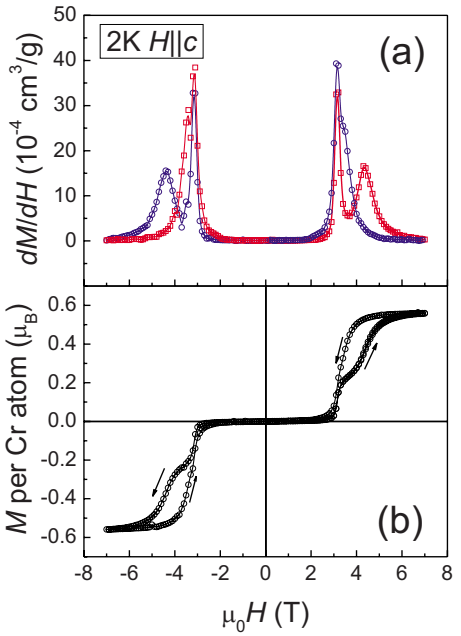

FIG. 4. (Color online) Magnetization M and its derivative with respect to the magnetic field, dM/dH, measured on CrOCl at $T=2$ K with the magnetic field applied along the **c** axis. The hysteresis in the magnetization branches with data collected by increasing and decreasing field (as indicated by the arrows) is clearly visible and symmetric if the field is reversed. (a) solid (red) lines and symbols □ mark values obtained on increasing the external field while (blue) solid lines and symbols ○ mark values obtained with decreasing external field.

creasing fields to be on the order of 1.3 T [Fig. 4(a)]. Combining the information obtained from magnetization and specific-heat experiments enables us to construct the (H,T) phase diagram for the magnetic phases of CrOCl as shown in Fig. 5.

B. X-ray diffraction

Preliminary x-ray diffraction experiments confirmed the FeOCl structure type of CrOCl. The first series of synchrotron experiments was carried out at selected temperatures in a cooling cycle from 270 to 9 K. At each temperature so-

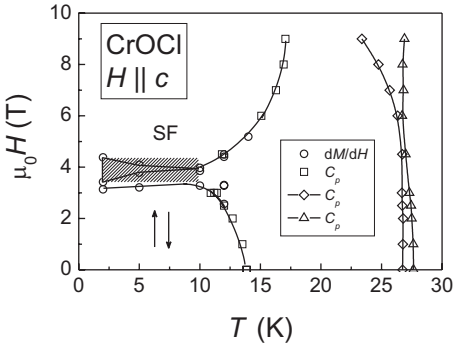

FIG. 5. Phase diagram of CrOCl with the magnetic field applied along the crystallographic **c** axis. The spin-flop phase is indicated by SF. The shaded area indicates the hysteresis of the spin-flop transition.

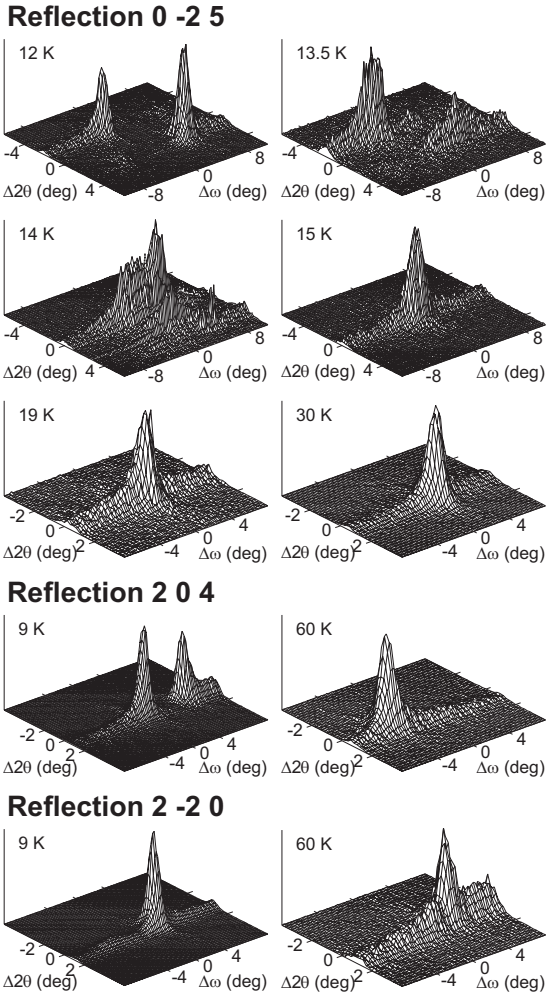

FIG. 6. Diffracted intensity as a function of the scattering angle 2θ and the crystal orientation ω for several reflections at selected temperatures. $\Delta 2\theta$ and $\Delta\omega$ indicate the deviation from the center of the scan in units of 0.01°.

called ω-2θ maps were measured for the reflections $(0\bar{2}5)$, (2 0 4), and $(2\bar{2}0)$. To this end, detector slits of 6×0.02 mm^2 were set, which correspond to an acceptance angle in the direction of 2θ of 0.0031°. ω scans (rotation of the crystal) were carried out for a series of 2θ values, with step sizes of 0.002° in both ω and 2θ. The resulting plot shows the diffracted intensity as a function of the orientation of the crystal and as a function of the scattering angle. Within the orthorhombic lattice all reflections are expected as single peaks, as is indeed observed down to $T=15$ K (Fig. 6). Some scans show a slight broadening of the peaks in the direction of ω, which indicates a less than optimal crystal quality, most likely resulting from anisotropic stress induced by different thermal contractions of the sample and the glue used to attach the sample.

At $T=9$ K the reflection $(0\bar{2}5)$ is split in both ω and θ while the reflection $(2\bar{2}0)$ remains sharp and (2 0 4) is split in ω only. These splittings imply a twinned monoclinic crystal with a monoclinic angle α different from 90°. Furthermore, they imply that the monoclinic distortion has occurred through a rotation of the **b** axis while the directions of the **a** and **c** axes are the same in both domains.

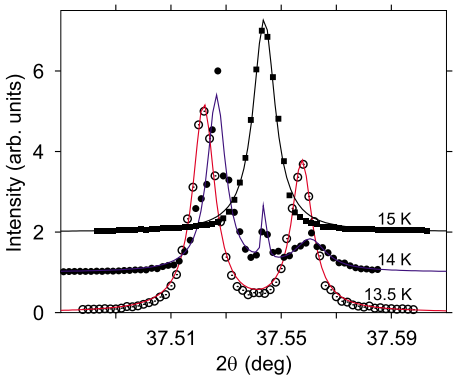

FIG. 7. (Color online) Diffracted intensity as a function of the scattering angle 2θ for the reflection $(0\bar{2}5)$ at selected temperatures. Lines represent fits to the data points with one, two, or three Lorentz-type functions at each temperature.

The experiment was continued by measuring ω-2θ maps of the $(0\bar{2}5)$ reflection by increasing the temperature in steps of 1 K. The splitting remained visible up to $T=13.5$ K and disappeared above $T=15$ K. At 14 K scattering centered at three different 2θ values was observed, which indicates the simultaneous presence of both the monoclinic low-temperature and the orthorhombic high-temperature phases. These observations prove that the transition at T_N is a first-order phase transition. At 13.5 K both maxima appear broadened in the direction of ω, suggesting that the transition might already have started. The transition temperature thus is estimated from the x-ray diffraction experiment as $T_N^{x\ ray}=13.5\pm0.5$ K, in good agreement with the magnetization and heat-capacity results.

Diffracted intensity as a function of scattering angle was obtained by summing the measured intensities of the ω-2θ maps in the direction of ω. By this we obtained pseudopowder-diffraction diagrams, which differ from real powder diffraction by the property that they do not contain diffraction by reflections other than $(0\bar{2}5)$ that might have similar scattering angles. Up to $T=13.5$ K these plots contain two maxima that can be well fitted with two Lorentzian functions (Fig. 7). The difference in the center positions of the two Lorentzians provide an accurate estimate for the splitting in 2θ from which the monoclinic angle α can be calculated.[19] The monoclinic distortion is weakly temperature dependent and corroborates the first-order character of the phase transition (Fig. 8).

At 9 K q scans were measured along **b** for six reflection pairs $(hkl)\rightarrow(hk+1l)$. These indicated the presence of superlattice reflections at half-integer k indices with the two highest intensities at (0 –0.5 3) and (2 –1.5 1). ω scans at these positions versus temperature showed the presence of superlattice reflections up to 13 K which disappeared above 15 K (Fig. 9).

IV. DISCUSSION

Preceding work has indicated a phase transition to occur in CrOCl at low temperatures toward a state with AFM order on a fourfold magnetic supercell.[8] Here we find that the AFM

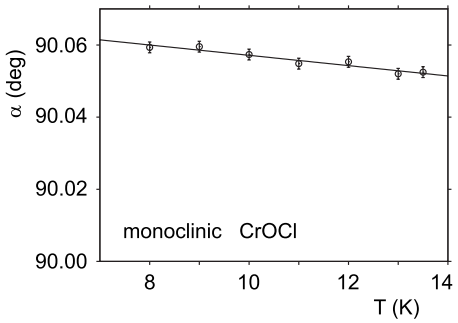

FIG. 8. Temperature dependence of the monoclinic angle α obtained from the splitting in 2θ of the reflection $(0\bar{2}5)$. The line represents a fit to the data points of $\alpha=\alpha_0+\alpha_T T$ with $\alpha_0=90.071(22)$ deg and $\alpha_T=-0.00143(18)$ deg/K.

phase transition is accompanied by a lattice distortion toward monoclinic symmetry and by a structural distortion toward a twofold, **2b**, nuclear superstructure. The transition occurs at $T_N=13.5$ K, which is significantly lower than the magnetic transition at ~80 K in VOCl. The magnitude of the lattice distortion ($\alpha=90.06°$ for CrOCl) is one third of that found in VOCl ($\gamma=90.2°$ for VOCl).[14,15] Both features indicate a sizeable magnetoelastic coupling in CrOCl which is, however, considerably weaker than in VOCl, despite the higher magnetic moment of Cr^{3+} compared to that of V^{3+}. An explanation for the different behaviors of CrOCl ($S=\frac{3}{2}$), VOCl ($S=1$), and TiOCl ($S=\frac{1}{2}$) can be found in the different symmetries of the filled $3d$ orbitals in these compounds.

The compounds MOCl (M=Ti, V, Cr) have a common topology and a common symmetry at the metal site. As a working hypothesis we therefore assume an equal hierarchy of $3d$-orbital energies. For TiOCl, calculated electronic band structures have been reported at various levels of

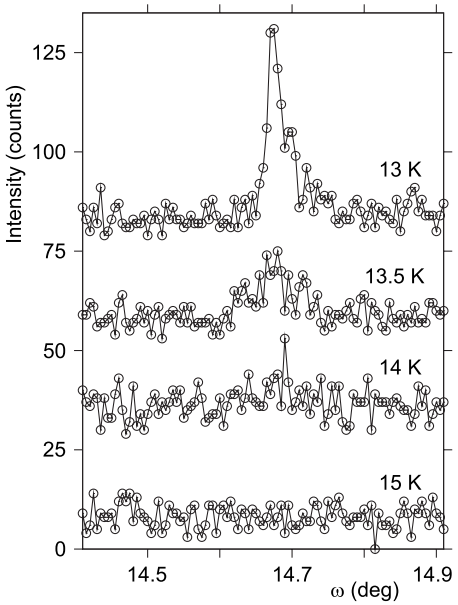

FIG. 9. ω scans centered at the superstructure reflection (2 –1.5 1) at selected temperatures. Given is the number of counts measured for 16 s in each step of 0.005° wide. Scans at consecutive temperatures have been given an incremental off-set of 25 counts.

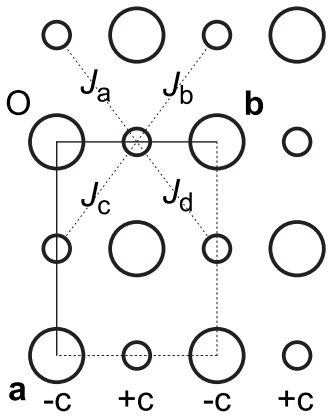

FIG. 10. Schematic representation of the *M*O double layers projected onto the a,b plane. Large circles denote oxygen atoms and small circles represent *M* atoms. The unit cell of room-temperature structure is indicated. $+c$ and $-c$ denote atoms located at different coordinates along **c**. A monoclinic distortion with $\gamma \neq 90°$ leads to exchange parameters $J_a = J_d \neq J_b = J_c$; a monoclinic distortion with $\alpha \neq 90°$ leads to $J_a = J_c \neq J_b = J_d$.

theory.[3,20,21] It has been found that the single valence electron of Ti^{3+} occupies the $3d_{x^2-y^2}$ orbital—for x along **b**, y along **c**, and z along **a**—that is responsible for AFM coupling by direct exchange between neighboring Ti atoms along **b**. The orbitals next higher in energy are $3d_{xz}$ and $3d_{yz}$.[3,20,21] These orbitals are empty in TiOCl. Here we assume that the two valence electrons of V^{3+} in VOCl occupy the $3d_{x^2-y^2}$ and $3d_{xz}$ orbitals[15] and that the three valence electrons of Cr^{3+} in CrOCl occupy the $3d_{x^2-y^2}$, $3d_{xz}$, and $3d_{yz}$ orbitals. This arrangement explains AFM coupling along **b** and strong exchange interactions between neighboring chains of metal atoms through the electrons in the $3d_{xz}$ and $3d_{yz}$ orbitals.

VOCl has been found to develop an **c**-axis unique monoclinic lattice distortion.[14,15] A closer inspection of the crystal structure suggests that this will be the most efficient lattice distortion in order to lift the degeneracy of exchange interactions on the *M*O bilayers involving the $3d_{xz}$ orbitals of V. This results in stripes of short $M-M$ contacts in the diagonal direction $\frac{1}{2}\mathbf{a}+\frac{1}{2}\mathbf{b}$ and stripes of long $M-M$ contacts in the direction $\frac{1}{2}\mathbf{a}-\frac{1}{2}\mathbf{b}$ (Fig. 10). AFM order along $\frac{1}{2}\mathbf{a}+\frac{1}{2}\mathbf{b}$ stripes then combines well with AFM order along **b** as imposed by direct exchange via the $3d_{x^2-y^2}$ orbitals. The result is AFM order along **a**. The same distortion also lifts the degeneracy of exchange interactions involving $3d_{yz}$ orbitals. However, AFM exchange interaction between these orbitals is probably enhanced along the direction $\frac{1}{2}\mathbf{a}-\frac{1}{2}\mathbf{b}$ of elongated bonds because σ-type overlap between $3d_{yz}$ orbitals on neighboring metal atoms is increased in this direction. It thus appears that an **c**-axis unique monoclinic distortion leads to frustration between exchange interactions via the $3d_{xz}$ orbitals (AFM interactions along $\frac{1}{2}\mathbf{a}+\frac{1}{2}\mathbf{b}$) and $3d_{yz}$ orbitals (AFM interactions along $\frac{1}{2}\mathbf{a}-\frac{1}{2}\mathbf{b}$). As both orbitals are occupied in CrOCl, the **c**-axis unique monoclinic distortion is unfavorable for this compound.

Experimentally, we have found an **a**-axis unique monoclinic lattice distortion for CrOCl, in agreement with the above interpretation. Structurally the easiest way to realize a distortion of this kind requires a relative shift of neighboring layers *M*OCl. However, this would hardly affect the frustrated exchange interactions within each layer. Instead, we have found that the monoclinic lattice distortion represents a shearing of individual layers, which then is responsible for the lifting of the degeneracy of exchange interactions on the *M*O double layers. Rotation of **b** in the (**b**,**c**) plane results in shorter *M*-*M* contacts that form a zigzag pattern on the average parallel to **a**. Direct exchange (AFM coupling) is increased along the shorter *M*-*M* contacts for both the $3d_{xz}$ and the $3d_{yz}$ orbitals. The result is a ferromagnetic arrangement along **a**, which might explain the predominant FM exchange as derived from Curie-Weiss temperature. This order can be combined by AFM coupling between neighboring *M* atoms along **b**. The role of the small structural distortion (doubling of the **b** axis) could be to increase the exchange interactions between the zigzag stripes, however a more detailed description requires a complete structure model of the low-temperature phase. It is noticed that nuclear superstructures with a wave vector that is twice the wave vector of the magnetic superstructure can be induced by the magnetic superstructure, as it has been explained theoretically.[22] Incidentally, applying the same reasoning to the twofold magnetic superstructure of VOCl, predicts the absence of a nuclear superstructure, in agreement with the experiment.[15]

The specific-heat data indicate additional transitions at a temperature of ~27.2 K (Fig. 3). A signature of this magnetic transition has not been found in our x-ray diffraction data while a weak anomaly is present in $\chi_M(T)$ (at the arrow in Fig. 2). This suggest a purely magnetic character of this transition, for example, the formation of incommensurate magnetic order.

While an **c**-axis monoclinic distortion appears to provide a maximum effect on lifting the degeneracy of the coupling between $3d_{xz}$ orbitals of metal atoms on neighboring ribbons, it does not do so for the $3d_{yz}$ orbitals. Instead, an **a**-axis monoclinic distortion through a change in direction of the **b** axis—i.e., representing a distortion of the layers rather than a relative shift between layers—accompanied by a structural distortion representing a doubling of the **b** axis leads to the required lifting of degeneracy of exchange interactions through the $3d_{yz}$ orbitals. The different lattice distortions of VOCl and CrOCl are thus explained by the different symmetries of the filled $3d$ orbitals.

V. CONCLUSIONS

The phase transition of CrOCl toward a state of AFM order has been identified as a first-order phase transition at $T_N = 13.5$ K, which is accompanied by a lattice and a structural distortion toward a twofold, 2**b** superstructure with **a**-axis unique monoclinic symmetry. The ordered magnetic moment is parallel to **c**. A second transition is discovered that is presumably of purely magnetic origin and might indicate the formation of an incommensurate magnetic superstructure.

The different behaviors of TiOCl, VOCl, and CrOCl result from different symmetries of the occupied $3d$ orbitals, which lead to different exchange interactions on the *M*O double layers of these isostructural series of compounds.

ACKNOWLEDGMENTS

Single crystals of CrOCl have been grown by A. Suttner. We gratefully acknowledge W. Morgenroth for assistance with the x-ray diffraction experiments with synchrotron radiation at Hasylab and E. Brücher and G. Siegle with magnetization and heat-capacity measurements. Financial support has been provided by the German Science Foundation (DFG).

*smash@uni-bayreuth.de; www.crystal.uni-bayreuth.de

[1] A. Seidel, C. A. Marianetti, F. C. Chou, G. Ceder, and P. A. Lee, Phys. Rev. B **67**, 020405(R) (2003).
[2] M. Shaz, S. van Smaalen, L. Palatinus, M. Hoinkis, M. Klemm, S. Horn, and R. Claessen, Phys. Rev. B **71**, 100405(R) (2005).
[3] T. Saha-Dasgupta, R. Valenti, H. Rosner, and C. Gros, Europhys. Lett. **67**, 63 (2004).
[4] H. Schäfer and F. Wartenpfuhl, Z. Anorg. Allg. Chem. **308**, 282 (1961).
[5] P. Ehrlich and H.-J. Seifert, Z. Anorg. Allg. Chem. **301**, 282 (1959).
[6] A. Haase and G. Brauer, Acta Crystallogr., Sect. B: Struct. Crystallogr. Cryst. Chem. **31**, 2521 (1975).
[7] M. D. Lind, Acta Crystallogr., Sect. B: Struct. Crystallogr. Cryst. Chem. **26**, 1058 (1970).
[8] A. N. Christensen, T. Johansson, and S. Quézel, Acta Chem. Scand. Ser. A **28**, 1171 (1975).
[9] A. Adam and G. Buisson, Phys. Status Solidi A **30**, 323 (1975).
[10] A. Wiedenmann, J. P. Venien, P. Palvadeau, and J. Rossat-Mignod, J. Phys. C **16**, 5339 (1983).
[11] S. van Smaalen, L. Palatinus, and A. Schonleber, Phys. Rev. B **72**, 020105(R) (2005).
[12] A. Krimmel, J. Strempfer, B. Bohnenbuck, B. Keimer, M. Hoinkis, M. Klemm, S. Horn, A. Loidl, M. Sing, R. Claessen, and M. v. Zimmermann, Phys. Rev. B **73**, 172413 (2006).
[13] A. Schönleber, S. van Smaalen, and L. Palatinus, Phys. Rev. B **73**, 214410 (2006).
[14] A. C. Komarek, T. Taetz, M. T. Fernandez-Diaz, D. M. Trots, A. Möller, and M. Braden, Phys. Rev. B **79**, 104425 (2009).
[15] A. Schönleber, J. Angelkort, S. van Smaalen, L. Palatinus, A. Senyshyn, and W. Morgenroth, Phys. Rev. B **80**, 064426 (2009).
[16] K. Nocker and R. Gruehn, Z. Anorg. Allg. Chem. **619**, 699 (1993).
[17] P. W. Selwood, *Magnetochemistry*, 2nd ed. (Interscience, New York, 1956).
[18] A. Abragam and B. Bleaney, *Electron Paramagnetic Resonance of Transition Ions* (Oxford University Press, Oxford, 1970).
[19] A. Schönleber, G. Shcheka, and S. van Smaalen, Phys. Rev. B **77**, 094117 (2008).
[20] D. Fausti, T. T. A. Lummen, C. Angelescu, R. Macovez, J. Luzon, R. Broer, P. Rudolf, P. H. M. van Loosdrecht, N. Tristan, B. Buchner, S. van Smaalen, A. Möller, G. Meyer, and T. Taetz, Phys. Rev. B **75**, 245114 (2007).
[21] Y.-Z. Zhang, H. O. Jeschke, and R. Valenti, Phys. Rev. Lett. **101**, 136406 (2008).
[22] S. W. Lovesey and S. P. Collins, *X-ray Scattering and Absorption by Magnetic Materials* (Clarendon, Oxford, 1996).